



Shear-thickening performance of suspensions of mixed ceria and silica nanoparticles

Minghai Wei^{1,3}, Li Sun^{2,3,*}, Chunwei Zhang⁴, Peipei Qi², and Jie Zhu²

¹Department of Construction and Engineering Management, Shenyang Jianzhu University, Shenyang, China

²School of Civil Engineering, Shenyang Jianzhu University, Shenyang, China

³School of Civil Engineering, Dalian University of Technology, Dalian, China

⁴School of Civil Engineering, Qingdao University of Technology, Qingdao, China

Received: 3 July 2018

Accepted: 28 August 2018

Published online:

5 September 2018

© Springer Science+Business Media, LLC, part of Springer Nature 2018

ABSTRACT

In this work, the shear-thickening (ST) performance of a novel suspension of ceria and silica mixed nanoparticles was systematically studied. Ceria/silica-shear-thickening fluids (CeO₂/SiO₂-STFs) of different concentrations were prepared by using an ultrasonication and mechanical stirring technique. The presence of ceria nanoparticles and their interaction with the SiO₂ nanoparticles in the STF were analyzed using scanning electron microscopy, energy-dispersive spectroscopy and X-ray diffractometry. Steady-shear rheological tests showed that distinct rheological behaviors and clear ST effects existed in CeO₂/SiO₂-STFs with different mass ratios. The viscosity increased from 50.97 (SiO₂-STF) to 111.51 Pa·s (CeO₂/SiO₂-STF), and the critical shear rate decreased from 63.09 to 19.95 s⁻¹ when the concentration of the ceria nanoparticles was 12 wt%. An oscillatory dynamic rheological analysis showed that the 12%CeO₂/20%SiO₂-STF suspension not only had significant energy storage and energy dissipation capacities but also presented excellent elastic behaviors when subjected to low stress and significant energy dissipation under high stress. The results also showed that the temperature exerted little influence on the viscosity of the CeO₂/SiO₂-STF suspension but had a significant influence on the ST effect. Furthermore, the current carried by the CeO₂/SiO₂-STF suspension increased with the increasing ceria nanoparticle content, indicating improved conductivity. This work provides a novel method for the production of high-performance STFs.

Address correspondence to E-mail: sunli2009@163.com

Introduction

A shear-thickening fluid (STF) is a nanocomposite non-Newtonian fluid formed by dispersing nanoparticles in a dispersant. Under normal conditions, STFs are slightly viscous liquids, but under exposure to a high shear rate such as from a high velocity or external impact, the viscosity, shear modulus and other rheological properties will increase significantly due to a “hydroclustering” mechanism, and the characteristics of STF are similar to those of a solid [1, 2]. Most importantly, once the impact is removed, the STF can return to its initial liquid state [3]. In this process, the STF absorbs a large amount of shock energy to induce a buffering and damping effect. Due to their shear-thickening (ST) effects, STFs are widely used as base materials such as fibers, fabrics and ceramic polymers in industry.

Many factors could affect the rheological properties of STFs, including the size and shape of the dispersed particles [4, 5], the mass fraction of the dispersed particles [6, 7], dispersion medium [8, 9] and environmental temperature [10–12]. Egres and Wagner [4] studied suspensions formed by anisotropic particles and found that in suspensions of large-sized particles, suspensions of rod-like particles are the most likely to be ST, followed by plate particles, while ball particles produce the smallest viscosity. The irregular shape of calcium carbonate particles in suspension also results in a more significant ST performance. Maranzano and Wagner [13] showed that (a) the higher the mass fraction of the dispersed-phase particles and the greater the initial viscosity of the system; (b) the more obvious the ST effect and the smaller the critical shear rate. Osman and Atalla [9] showed that the interaction between the particles and dispersing medium is connected to the molecular chains and functional groups of polymers, causing the changes in the dispersion’s performance. Wagner et al. [11] conducted a detailed experimental study on the temperature sensitivity of STFs and found that the initial viscosity, minimum viscosity and peak viscosity decreased with the increasing ambient temperature. However, due to the extensive aggregation of nanoparticles, it is difficult to obtain a suspension system with a more significant ST effect by increasing the mass fraction of a single type of dispersed-phase particle in most STF preparation processes [14]. Therefore, researchers have prepared

many new series of STF systems by using chemical or physical methods to add functional groups to the dispersed-phase structure and to disperse the resulting material into special liquids [15–20].

Yang et al. [21] studied the ST phenomenon in TiO_2 particle suspensions. They found that if the particle size distribution of the TiO_2 particles was wide, the viscosity and yield stress of the particles would be reduced. Mixing dispersed particles of different sizes can result in an effective STF, and the particle ratio and particle size ratio will also cause significant effects on the properties. Hwang et al. [22] added multi-walled carbon nanotube (MWCN) powders to a SiO_2 /PEG suspension and found that the ST effect was greatly improved due to the excellent mechanical properties of the MWCN powder and the good dispersibility of the silica particles. The rheology of STFs with various ceramic particle additives, such as silicon carbide, aluminum oxide and boron carbide, under various temperatures, were experimentally investigated by Gürgen et al. [19] They found that the suspensions exhibited different systematic variations with respect to the varied parameters. To enhance the sound insulation performance of an STF-fabric, Wang et al. [23] prepared a compound STF with tetrapod ZnO whiskers, (TW-ZnO)/ SiO_2 . The results showed that the ST effect of TW-ZnO/ SiO_2 could be better than that of SiO_2 -STF, and the sound insulation performance of the STF-fabric is superior to that of the original fabric. Sha et al. [14] found that CNTs could improve the ST performance, while GNs would reduce the viscosity of the suspension. When the mass fractions of the two were 2% and 1%, the suspension showed a good ST effect. Chen et al. [24] added carbon nanotubes (CNTs) into SiO_2 -STF, and not only was the ST effect strengthened with the increasing CNT mass fraction, but the suspension also had a unique conductivity. Qin et al. [25] systematically studied suspensions formed by ionic liquids and hydrophilic silicas. The results showed that the use of ionic liquids with different structures could change the rheological and viscoelastic characteristics of the suspension. Jiang et al. [26] investigated the dispersion system of poly (methyl methacrylate)-glycerol-water and found that the viscosity of the dispersed medium decreased with the decreasing water content. The critical shear rate of the STF increased, and the ST was inhibited. The above studies indicate that the use of different dispersed

particles causes different effects on the physical properties of the STFs.

To improve the ST behaviors of silica suspensions and obtain multifunctional materials, tombarthite ceria is chosen in our study. Tombarthite functional materials have received increasing interest in material science [27–30]. They are widely used as ceria nanoparticles in suspensions, alloys and ceramic composites to improve the optical, electrical, and stability properties of the carriers, especially the thermal stability and aging resistance for polymer fibers and coatings. In this work, tombarthite ceria nanoparticles are characterized and dispersed into PEG to prepare STFs. The ST (ST) performance of the suspension is evaluated by both steady-shear and oscillatory-shear testing, and the influences of the mass fraction of the ceria nanoparticles and the environmental temperature on the ST performance of the suspensions are carefully investigated.

Experiment

Materials

The silica nanoparticles used in this study are a type of hydrophilic gas-phase silica and were obtained from Degussa Company (China). Their primary particle size and pH value are 12 nm and 3.7–4.7, respectively. The polyethylene glycol (PEG200), obtained from Qingdao Yousuo Chemical Technology Co., Ltd. (China), has a hydroxyl value of 510–623 mgKOH/g, and it is a stable transparent liquid at room temperature. The dispersant is N-(3-triethoxysilylpropyl)-ethylenediamine with a molecular weight of 222.36. The ceria nanoparticles are purchased from Shanghai Macklin Biochemical Technology Co., Ltd. (China). Their purity and average particle size are 99.5% and 20 nm, respectively. The normal condition is a pale yellow powder.

Preparation of concentrated suspensions

Before the test, the dispersed-phase particles were moved to a vacuum drying oven and dried at a constant temperature of 80 °C for 12 h. In the process of preparation, a certain amount of PEG200 and additives (approximately 2% of the mass fraction of the dispersed phase) were added to a beaker. The solution was evenly mixed by stirring the solution

with a mechanical agitator. Then the calculated masses of silica and ceria nanoparticles were gradually added into the solution. In this process, an ultrasonic oscillator was continuously used, and a constant-temperature water bath was provided for the stirred beaker. After the powder was added, the dispersing phase was stirred and oscillated until the dispersed-phase particles were dispersed uniformly in the PEG200. Finally, the configured suspension was placed in the vacuum drying oven at 110 °C to remove the bubbles to generate CeO₂/SiO₂-STF, which is shown in Fig. 1.

Rheological and electrochemical tests

The steady-state and dynamic flow properties of CeO₂/SiO₂-STFs with different mass ratios were measured using an AR2000 rheometer (TA Instruments, USA) at 25 °C. The diameter of the flat rotor and the plate spacing were 25 mm and 0.1 mm, respectively. An electrochemical performance experiment with different mass mix ratios were carried out by using the EC705 modular electrochemical analysis system that was purchased from Wuhan Gaoss Union Technology Co., Ltd. (China) at a scanning rate of 10 mV/s. Ruthenium iridium oxide was used as the working electrode, iridium titanium oxide was used as the auxiliary electrode, and a saturated calomel electrode was used as the reference electrode.

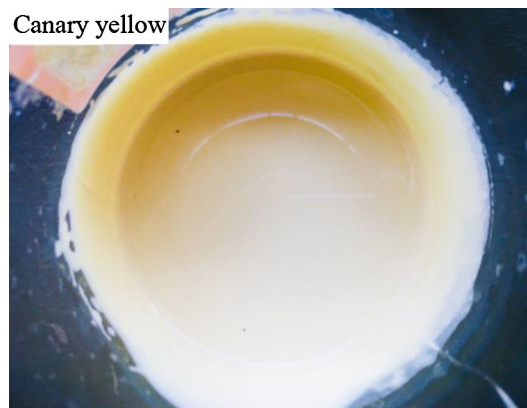


Figure 1 STF has been made by CeO₂ and SiO₂ nanoparticles.

Results and discussion

Physical characterization

Appropriate amounts of silica, ceria and $\text{CeO}_2/\text{SiO}_2$ samples were mixed with ethanol and dispersed evenly with ultrasonic waves. Then, the liquid was removed from the copper foil for drying. The morphology of these samples was analyzed by using a scanning electron microscope (SEM, S-4800) at acceleration 20 kV, and the results are shown in Fig. 2.

Figure 2a shows that the particle size of the silica nanoparticles is small and that the surface area is large. The agglomeration phenomenon is serious, and the degree of particles' monodispersity is high. Therefore, a dispersing agent should be added in the STF to improve the dispersion of the silica nanoparticles and enhance the ST behavior. As can be seen from Fig. 2b, the ceria nanoparticles are also spherical with a uniform particle size and regular morphology. The shape and size of the ceria nanoparticles are essentially the same as those of the silica nanoparticles. Figure 2c is a SEM image of the mixed silica and ceria nanoparticles; it shows that the ceria nanoparticles are easily combined with the silica nanoparticles and distributed in blocks.

To verify the constitution of the $\text{CeO}_2/\text{SiO}_2$ sample, energy-dispersive spectroscopy (EDS) mapping was analyzed. The EDS scan region of the $\text{CeO}_2/\text{SiO}_2$ sample is shown in Fig. 3a. The sample has some concave and convex surfaces, and thus, its surface is not smooth, indicating the clustering of particles. The corresponding plane scan results of the O, Si and Ce elements are shown in Fig. 3b. All of the elements are non-uniformly distributed on the surface, and there is

some enrichment phenomenon for all three elements. The mass fractions of the chemical elements on the sample (wt%) are O 85.78, Si 39.39 and Ce 22.37, and the atomic fractions (at%) are O 77.44, Si 20.26 and Ce 2.31, as shown in Fig. 3c. The atomic ratio is approximately 1:0.26:0.03. Hence, the sample is composed of SiO_2 and CeO_2 .

An X-ray diffractometer (XRD, ARL XTRA, Thermo Electron) was used to analyze the characteristics of the different samples using Cu target radiation. The voltage and current of the test were 40 kV and 30 mA, respectively. The angle range and speed of the scanning were 5° – 90° and 8 degree/min, respectively. The step length was 0.04 degrees. The test results are shown in Fig. 4.

Figure 4 shows, for the silica sample, a “steamed bread” peak with a wide distribution in the diffraction angle region between 15° and 25° . With the increasing diffraction angle, the diffraction intensity gradually decreases and eventually becomes stable, indicating that the silica samples are amorphous. On the other hand, the diffraction peaks of the ceria samples are clear and sharp and the position of the characteristic peak is consistent with the spectrum of the ceria standard card (JCPDS card 34-0394). These results show that the ceria samples have a fluorite-type face-centered cubic structure, which belongs to the $\text{Fm}\bar{3}m$ space group. The XRD of the ceria samples shows no other peaks such as oxides and hydroxides of cerium, indicating that the ceria samples have no such components in their crystalline form. The diffraction peak distribution in Fig. 4 is more consistent with that of ceria samples, but the strength is decreased. This shows that the mixed sample contains ceria crystals.

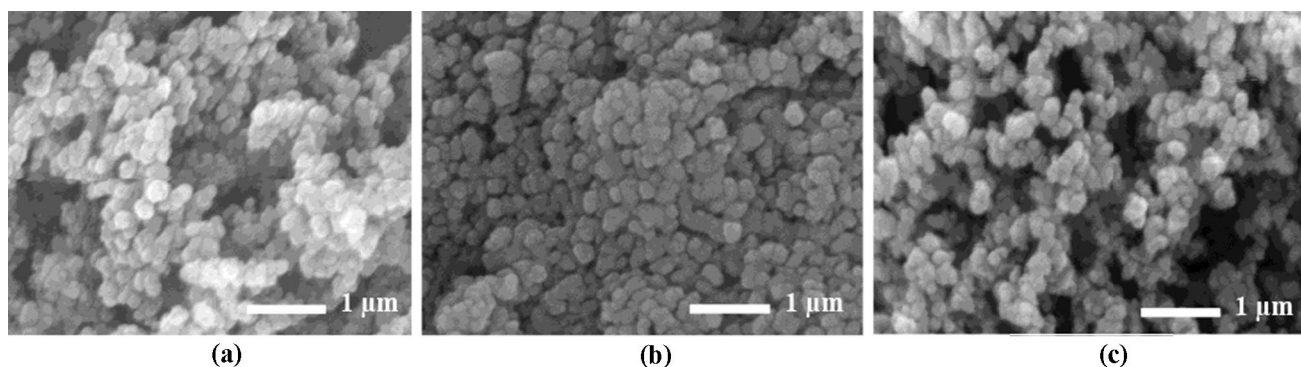


Figure 2 SEM images of different nanoparticles. **a** Silica. **b** Ceria. **c** $\text{CeO}_2/\text{SiO}_2$.

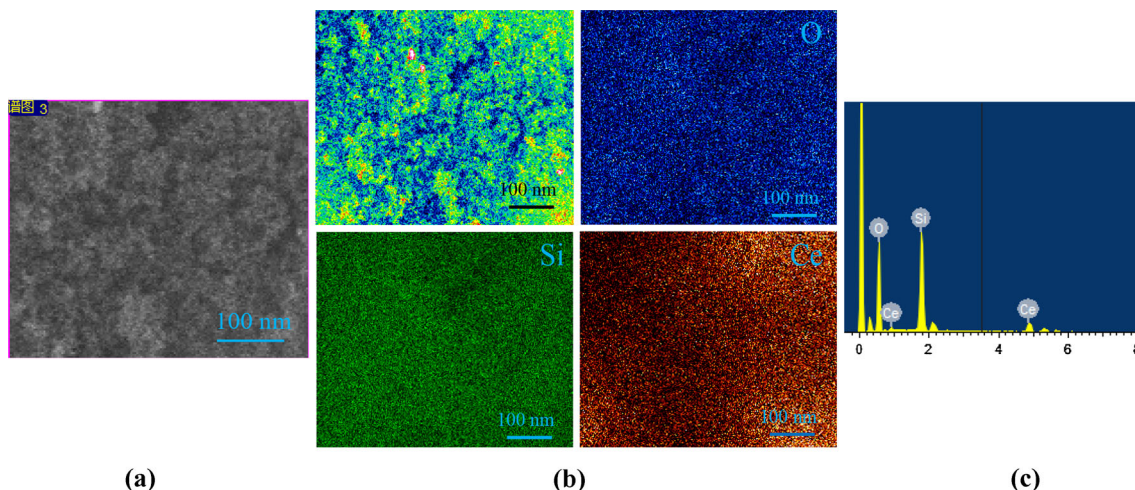


Figure 3 EDS mapping analysis for the $\text{CeO}_2/\text{SiO}_2$ sample (mass ratio is 1:1). **a** EDS scan region. **b** EDS mapping results. **c** EDS spectrum.

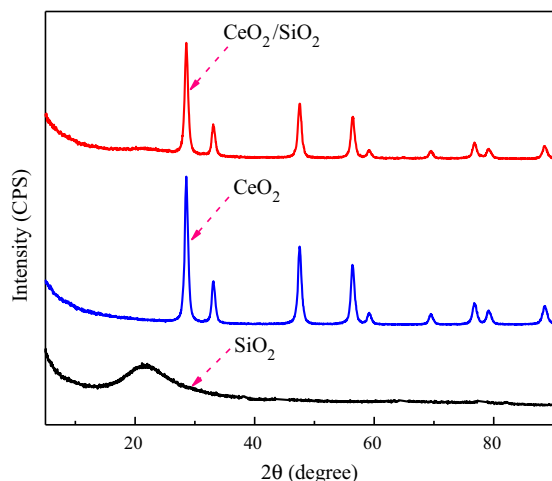


Figure 4 XRD patterns of different nanoparticles.

Steady-shear rheological properties

Figure 5 shows the viscosity curves of the $\text{CeO}_2/\text{SiO}_2$ -STF with five different mass mixture ratios under the steady-state test in the shear rate range of $0.1\text{--}1000\text{ s}^{-1}$. The dispersive medium for all samples was PEG200. On the basis of 20% SiO_2 -STF, the mass fraction of CeO_2 was 0%, 6%, 12%, 15% and 20%, respectively. The initial point, critical ST point and peak point coordinates of the viscosity of each system are shown in Table 1. As seen in Fig. 5, all the curves contain a shear-thinning area, a shear-thickening area, and a rapid decline area after reaching the peak viscosity within the testing limit. However, there is no evident relationship between the mass fraction of

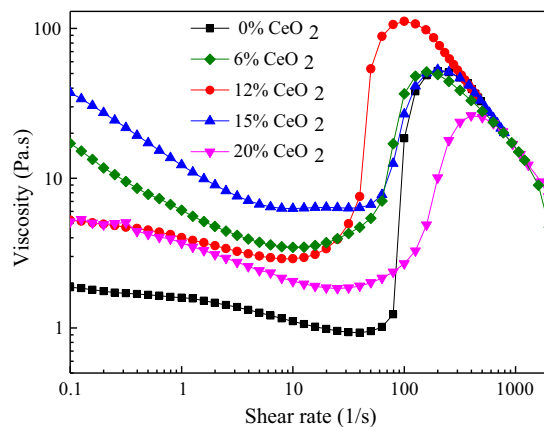


Figure 5 Viscosity versus shear rate for the $\text{CeO}_2/\text{SiO}_2$ -STF suspension with various $\text{CeO}_2\text{--SiO}_2$ ratios.

CeO_2 and the viscosity changes in the shear-thinning and shear-thickening areas.

Compared with SiO_2 -STF, the critical shear rate of 6% CeO_2 was reduced significantly from 50.0 to 12.59 s^{-1} , and the initial viscosity increased 35 times to $66.54\text{ Pa}\cdot\text{s}$ with a nearly identical peak viscosity. The possible explanations are as follows: When a small amount of CeO_2 particles was added to the SiO_2 -STF system, the overall number of particles within a unit volume of the suspension system increased, decreasing the distance between particles. Therefore, the chance of particle contact increased and agglomeration was promoted, which increased the flow friction. This was shown as a significant increase in the initial viscosity. On the other hand, the addition of a small amount of CeO_2 improved the

Table 1 Key coordinates of different CeO₂/SiO₂-STF

CeO ₂ /SiO ₂ -STF suspension	Initial point	Critical ST point	Peak point
0% CeO ₂ + 20% SiO ₂	0.12 s ⁻¹ , 1.84 Pa·s	50.0 s ⁻¹ , 0.95 Pa·s	199.65 s ⁻¹ , 51.95 Pa·s
6% CeO ₂ + 20% SiO ₂	0.12 s ⁻¹ , 66.54 Pa·s	12.59 s ⁻¹ , 3.47 Pa·s	158.57 s ⁻¹ , 51.28 Pa·s
12% CeO ₂ + 20% SiO ₂	0.12 s ⁻¹ , 6.08 Pa·s	12.59 s ⁻¹ , 2.95 Pa·s	100.10 s ⁻¹ , 111.51 Pa·s
15% CeO ₂ + 20% SiO ₂	0.12 s ⁻¹ , 27.38 Pa·s	39.81 s ⁻¹ , 6.35 Pa·s	199.68 s ⁻¹ , 53.09 Pa·s
20% CeO ₂ + 20% SiO ₂	0.12 s ⁻¹ , 4.03 Pa·s	39.81 s ⁻¹ , 1.91 Pa·s	398.40 s ⁻¹ , 26.23 Pa·s

gradation of particles in the suspension, reducing the space between particles as well as the distance between surfaces with an increased mean particle diameter. Therefore, in the low shear rate range (< 10 s⁻¹), the larger hydrodynamic force of the water induced an intense coupling reaction among particles in short range, which rapidly increased the viscosity in the system due to the “particle-cluster effect.” Meanwhile, in the high shear rate range (approximately 100 s⁻¹), the peak viscosity barely changed, likely due to the weak bonding between the CeO₂ and SiO₂ particles.

When the mass fraction of CeO₂ was increased to 12%, the critical shear rate remained the same as in the 6% CeO₂ system (12.59 s⁻¹). Nonetheless, the initial viscosity of the suspension decreased significantly to 6.08 Pa·s, indicating improved rheology. More importantly, the peak viscosity increased two times to 111.51 Pa·s, with a shift to a lower shear rate. This could be attributed to a better gradation formed by 12% CeO₂ and 20% SiO₂ particles with a superior dispersion as well as a larger and more evenly distributed space between particles. In addition, a larger diameter and a higher mass density of agglomerates resulted in a substantial increase in the ST effect for this particular mixture ratio [7, 31].

It should be noted that when the mass fraction of CeO₂ was further increased to 15%, the CeO₂/SiO₂-STF system showed significant decreases in the flowability, critical shear rate and peak viscosity (as shown in Table 1). This might be attributed to the excessive amount of CeO₂ within the system filling up the space between agglomerates and inhibiting the flow. As for the shear-thickening mechanism, an underdeveloped cluster effect caused by poor gradation resulted in a higher critical shear rate. Interestingly, when the mass fraction of CeO₂ was increased to 20%, the critical shear rate for the system remained approximately unchanged (39.81 s⁻¹), with an overall downward shift in the viscosity of approximately 50% and an approximately 200%

increase in the corresponding shear rate. This observation indicates that once the mass fraction of CeO₂ passes a certain threshold, the ST effect of the system is weakened. However, the further decrease in the initial viscosity indicates that the rheology of the system is improved. This might be attributed to the high mass density composites formed by SiO₂-STF and PEG200, and the CeO₂ particles are only dispersed in the continuous composites. Before a cluster structure was formed by the CeO₂ and SiO₂ particles, the system demonstrated good rheology due to the high mass density.

Dynamic shear rheological response

An analysis of Fig. 5 shows that when the mass fraction of ceria nanoparticles is 12%, the CeO₂/SiO₂-STF system has good fluidity and the shear-thinning behavior is not clearly observed. It is more important that the critical shear rate that inspires the ST effect of the STF is low, and the peak viscosity is not only high but increases quickly. Thus, this STF can be used as an energy dissipation medium in dampers or isolators in the fields of vibration control and structural aseismic design. Therefore, Fig. 6 further details the behavior of the 12%CeO₂/20%SiO₂-STF at fixed angular frequencies of 10 rad/s, 20 rad/s, 40 rad/s and 80 rad/s for the energy storage modulus (G') and the energy dissipation modulus (G'') with the increase in the strain. Figure 7 shows the G' and G'' behaviors with the angular frequency increasing under fixed strains of 75%, 150%, 300% and 600%.

Figure 6 shows that the 12%CeO₂/20%SiO₂-STF system went through four stages: a linear elastic stage, weak shear-thinning stage, strong shear-thickening stage, and secondary shear-thinning stage (failure stage). As the angular frequency increased from 10 to 80 rad/s, the curves of G' and G'' both demonstrated overall upward shifts with a decreased critical oscillation strain. This was attributed to the

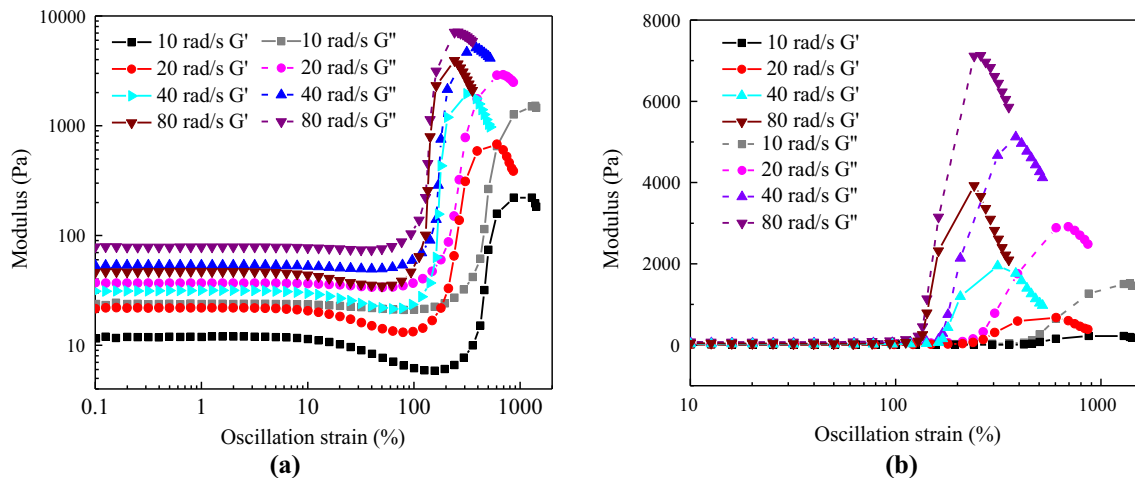


Figure 6 Storage and loss modulus versus strain for 12%CeO₂/20%SiO₂-STF. **a** Logarithmic coordinate. **b** Semi-logarithmic coordinate.

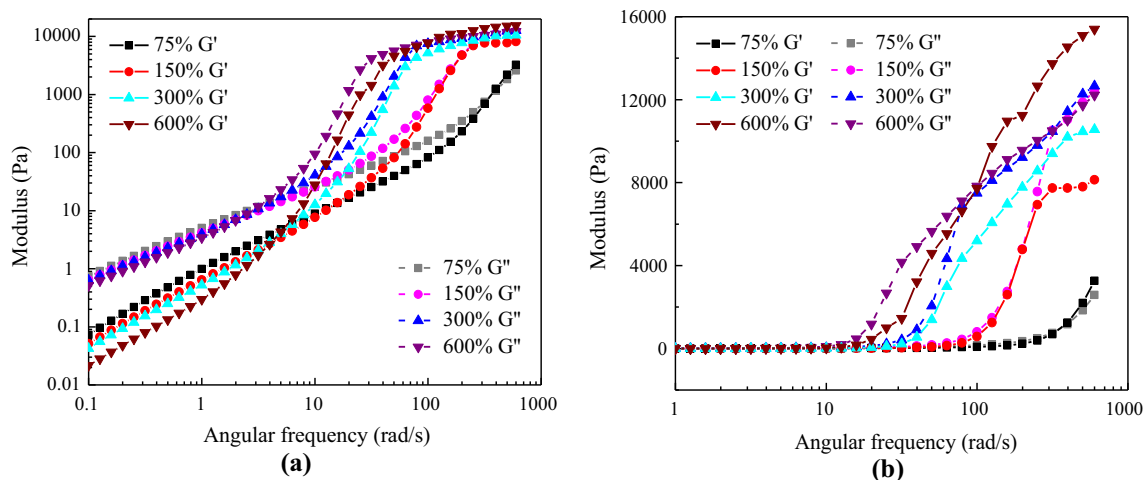


Figure 7 Response of storage and loss modulus against frequency for 12%CeO₂/20%SiO₂-STF. **a** Logarithmic coordinate. **b** Semi-logarithmic coordinate.

favorable environment created for the particle clusters within the system by the even distribution of the particles induced by the increment of the angular frequency. A closer look at Fig. 6a, b shows that G'' is always greater than G' at different angular frequencies, particularly as the angular frequency increases. In addition, as the angular frequency decreases and the strain approaches the critical point, the curves of G' show but a slight decrease and those of G'' remained flat, which indicates that no significant shear thinning occurred to this specific STF system with high instantaneous energy dissipation.

Figure 7 shows the responses of the storage and loss moduli against frequency for 12%CeO₂/20%SiO₂-STF. It can be seen that with the increment of the strain magnitude, both the G' and G'' curves

display a similar trend: (1) a high non-linear spike of the modulus curves as the angular frequency increases and (2) a substantial decrease in the critical angular frequency. It is speculated that under a low angular frequency, the Brownian force and intermolecular force could promptly restore the damaged structure so that both G' and G'' remain unchanged or display slow linear increments. However, when the angular frequency was increased to a critical value, the hydro-lubrication of the suspension equilibrated with the Brownian and intermolecular forces combined and the system reached its critical shear rate. Beyond this point, hydro-lubrication would dominate and facilitate the formation of clusters to the extent that both G' and G'' non-linearly increase due to the impeded flow in the system. As shown in

Fig. 7b, when the strain magnitude is increased from 75 to 600%, the critical angular frequencies of G'' are 199.53 rad/s, 63.10 rad/s, 25.12 rad/s and 12.58 rad/s, with successive decreases of 136.43 rad/s, 39.98 rad/s and 12.54 rad/s. This reveals that this specific STF system has not only the capacity for significant ST under low frequency but also superior energy dissipation under high strain.

Temperature sensitivity

Figure 8 shows the relationship between the composite viscosity and the strain amplitude at different test temperatures for the 12%CeO₂/20%SiO₂-STF. The environmental test temperatures are 6.25 °C, 12.5 °C, 25 °C and 50 °C. The scanning angular frequency is constant at 20 rad/s, and the scanning range of the strain amplitude is 0.1–2000%.

As shown in Fig. 8a, the temperature variation has a similar effect on the complex viscosity for the 12%CeO₂/20%SiO₂-STF system and SiO₂-STF system [10]. As the temperature increases, the complex viscosity curves tend to shift downward with a decrease in the initial and peak viscosities as well as an increase in the critical shear rate. It is worth mentioning that the 12%CeO₂/20%SiO₂-STF system showed superior stability at all tested temperatures, without shear thinning before the critical shear strain. However, this does not translate to superior thermal stability. This is because the ST effect is significantly affected when the temperature rises. For instance, the peak complex viscosity is 478.32 Pa·s at 6.25 °C and the corresponding critical strain is 62.14%; when the

temperature rises to 12.5 °C, the peak complex viscosity is decreased 2.23 times with a 58% increased critical strain; when the temperature reaches 50 °C, as shown in Fig. 8a, the initial viscosity of the system displays a relatively significant decrease, and the complex viscosity fails to reach its peak within the testing limits, which indicates a weak ST effect. This might be attributed to a stronger repulsion between SiO₂ and CeO₂ particles under the higher temperature, in that case the hydrogen bond between SiO₂ and PEG is broken, producing an unfavorable environment for the formation of particle clusters within the suspension. Therefore, the particles from the shear-thickening system are evenly distributed within the PEG, which maintains the system's good rheology and a relatively low complex viscosity.

Electrochemical behavior

Figure 9 shows cyclic voltammetric curves of CeO₂/SiO₂-STFs with different mass ratios. It can be seen that the volt-ampere curve of a single SiO₂-STF almost coincides with the voltage's increasing and decreasing stages, indicating that the STF is an irreversible electrode. On the other hand, the two volt-ampere curves of the voltage increasing and decreasing stages have almost no encircling area, indicating that the capacitance and current are rather small. Therefore, it is considered that the single SiO₂-STF is almost non-conductive. However, the area of the two volt-ampere curves at the increasing and decreasing stages increases gradually with the increasing ceria mass fraction, indicating that the

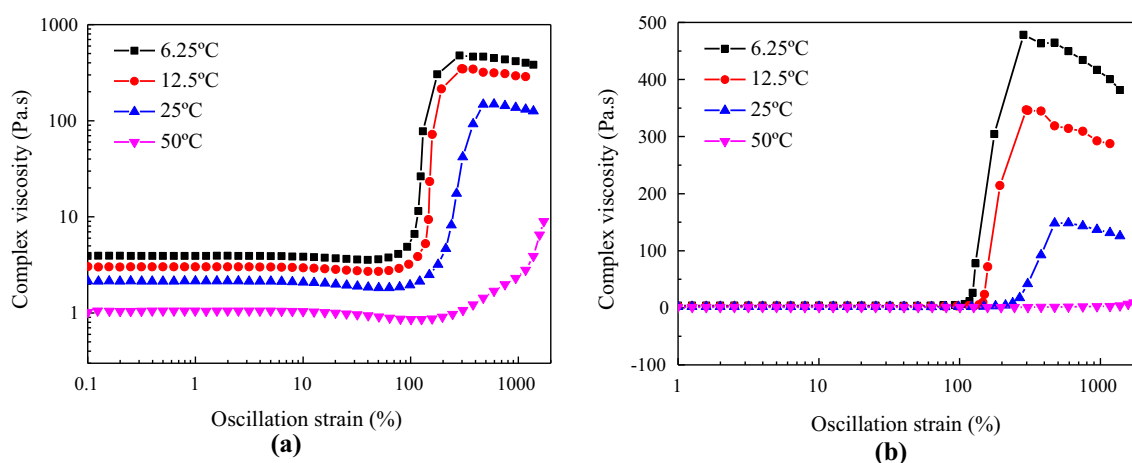


Figure 8 Complex viscosity versus oscillation strain for 12%CeO₂/20%SiO₂-STF at various temperatures. **a** Logarithmic coordinate. **b** Semi-logarithmic coordinate.

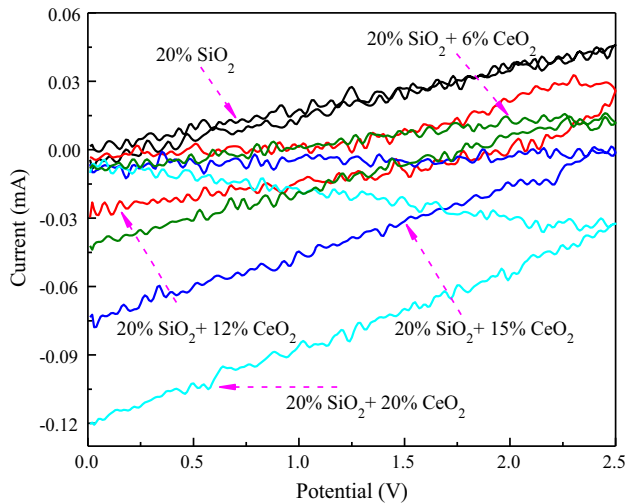


Figure 9 Effect of mass ceria content on the volt–ampere curve.

capacity and current of the STF increase gradually. It is more important that the behavior of the volt–ampere curve in the corresponding STF becomes more and more symmetrical in the phases of the voltage increasing and voltage decreasing, indicating that the STF electrode becomes reversible from being irreversible. Therefore, this STF may be used as a functional material due to its good conductivity.

Conclusion

In this study, $\text{CeO}_2/\text{SiO}_2$ -STF suspensions with different mass ratios were prepared and tested. This involved microscopic characterizations and investigations of the steady rheological properties and dynamic rheological response, as well as the temperature sensitivity and electrochemical behavior. The results showed that (a) the different mixture ratios of the $\text{CeO}_2/\text{SiO}_2$ -STF suspension had excellent ST performance, especially at shear rates less than the critical shear rate; (b) the addition of ceria nanoparticles significantly improved the apparent viscosity value of the SiO_2 -STF suspension. However, the effect of the ceria nanoparticles on the shear-thickening effect was not monotonic. When the mass fraction was 12%, the shear-thickening performance of the suspension was the best. For this sample, the critical shear rate of the $\text{CeO}_2/\text{SiO}_2$ -STF suspension was relatively small and the apparent viscosity peak was large. The results also showed that when the shear-thickening effect occurred in the 12% $\text{CeO}_2/20\%\text{SiO}_2$ -STF suspension, the increase in temperature had a

significant influence on the critical shear rate and the peak value of the complex viscosity; but the complex viscosity was almost invariant when the shear-thickening phenomenon was not occurring. This indicates that the suspension has reduced the influence of temperature to some extent. Moreover, ceria nanoparticles have a significant effect on the electrochemical performance of silica STFs. With the increase in the ceria content, not only did the current of the $\text{CeO}_2/\text{SiO}_2$ -STF increase significantly, but the STF electrode became reversible from being irreversible.

Acknowledgements

The authors acknowledge financial support from National Natural Science Foundation of China (Grant Nos. 51578347, 51608335), Natural Science Foundation of Liaoning Province (Grant No. 2015020578) and Basic scientific research projects of Liaoning Colleges and Universities (Grant No. LJZ2017045).

References

- [1] Tian T, Nakano M (2017) Design and testing of a rotational brake with shear thickening fluids. *Smart Mater Struct* 26(3):035038
- [2] Eric B, Heinrich MJ (2014) Shear thickening in concentrated suspensions: phenomenology, mechanisms and relations to jamming. *Rep Prog Phys* 77(4):046602
- [3] Waitukaitis SR, Jaeger HM (2012) Impact-activated solidification of dense suspensions via dynamic jamming fronts. *Nature* 487(7406):205–209
- [4] Egres RG, Wagner NJ (2005) The rheology and microstructure of acicular precipitated calcium carbonate colloidal suspensions through the shear thickening transition. *J Rheol* 49(3):719–746
- [5] Barnes HA (1989) Shear-thickening (“Dilatancy”) in suspensions of nonaggregating solid particles dispersed in Newtonian liquids. *J Rheol* 33(2):329–366. <https://doi.org/10.1122/1.550017>
- [6] Kamibayashi M, Ogura H, Otsubo Y (2008) Shear-thickening flow of nanoparticle suspensions flocculated by polymer bridging. *J Colloid Interface Sci* 321(2):294–301
- [7] Maranzano BJ, Wagner NJ (2001) The effects of interparticle interactions and particle size on reversible shear thickening: hard-sphere colloidal dispersions. *J Rheol* 45(5):1205–1222
- [8] Li C, Jiang H, Wang Y, Wang Y (2011) Hyperbranched poly(methyl methacrylate)s prepared by miniemulsion

- polymerization and their (non)-Newtonian flow behaviors. *Polymer* 52(2):376–382
- [9] Osman MA, Atallah A (2006) Interfacial adhesion and composite viscoelasticity. *Macromol Rapid Commun* 27(16):1380–1385
- [10] Tian T, Peng G, Li W, Ding J, Nakano M (2015) Experimental and modelling study of the effect of temperature on shear thickening fluids. *Korea-Aust Rheol J* 27(1):17–24
- [11] Wagner NJ, Brady JF (2009) Shear thickening in colloidal dispersions. *Phys Today* 62(10):27–32
- [12] Liu X-Q, Bao R-Y, Wu X-J, Yang W, Xie B-H, Yang M-B (2015) Temperature induced gelation transition of a fumed silica/PEG shear thickening fluid. *RSC Adv* 5(24):18367–18374
- [13] Maranzano BJ, Wagner NJ (2001) The effects of particle size on reversible shear thickening of concentrated colloidal dispersions. *J Chem Phys* 114(23):10514–10527
- [14] Sha X, Yu K, Cao H, Qian K (2013) Shear thickening behavior of nanoparticle suspensions with carbon nanofillers. *J Nanopart Res* 15(7):1816. <https://doi.org/10.1007/s11051-013-1816-x>
- [15] Qin J, Zhang G, Shi X, Tao M (2015) Study of a shear thickening fluid: the dispersions of silica nanoparticles in 1-butyl-3-methylimidazolium tetrafluoroborate. *J Nanopart Res* 17(8):333. <https://doi.org/10.1007/s11051-015-3144-9>
- [16] Qin J, Zhang G, Shi X (2016) Viscoelasticity of shear thickening fluid based on silica nanoparticles dispersing in 1-butyl-3-methylimidazolium tetrafluoroborate. *J Dispers Sci Technol* 37(11):1599–1606
- [17] Moosavi M, Daneshvar A (2014) Investigation of the rheological properties of two imidazolium-based ionic liquids. *J Mol Liq* 190:59–67
- [18] Novak J, Britton MM (2013) Magnetic resonance imaging of the rheology of ionic liquid colloidal suspensions. *Soft Matter* 9(9):2730–2737
- [19] Gürgen S, Li W, Kuşhan MC (2016) The rheology of shear thickening fluids with various ceramic particle additives. *Mater Des* 104:312–319
- [20] Wang F-F, Zhang Y, Zhang H, Xu L, Wang P, C-b Guo (2018) The influence of graphene nanoplatelets (GNPs) on the semi-blunt puncture behavior of woven fabrics impregnated with shear thickening fluid (STF). *RSC Adv* 8(10):5268–5279
- [21] Yang H-G, Li C-Z, Gu H-C, Fang T-N (2001) Rheological behavior of titanium dioxide suspensions. *J Colloid Interface Sci* 236(1):96–103
- [22] Hwang H, Lee J, Kim Y, Kim Y (2009) Preparation of silica-coated MWNTs and their addition to shear thickening fluid of silica/PEG suspension. In: 18th international conference on composite materials, 2009
- [23] Wang Y, Zhu Y, Fu X, Fu Y (2015) Effect of TW-ZnO/SiO₂-compounded shear thickening fluid on the sound insulation property of glass fiber fabric. *Text Res J* 85(9):980–986
- [24] Chen Q, Liu M, Xuan S, Jiang W, Cao S, Gong X (2017) Shear dependent electrical property of conductive shear thickening fluid. *Mater Des* 121:92–100
- [25] Qin J, Zhang G, Ma Z, Li J, Zhou L, Shi X (2016) Effects of ionic structures on shear thickening fluids composed of ionic liquids and silica nanoparticles. *RSC Adv* 6(85):81913–81923
- [26] Jiang W, Sun Y, Xu Y, Peng C, Gong X, Zhang Z (2010) Shear-thickening behavior of polymethylmethacrylate particles suspensions in glycerine–water mixtures. *Rheol Acta* 49(11–12):1157–1163
- [27] Lee S, Shin D, Park M, Hong J, Kim H, Son JW, Lee JH, Kim BK, Lee HW, Yoon KJ (2016) Highly controlled thermal behavior of a conjugated gadolinia-doped ceria nanoparticles synthesized by particle-dispersed glycine–nitrate process. *J Eur Ceram Soc* 37(5):2159–2168
- [28] Biesuz M, Spiridigliozzi L, Frasnelli M, Dell’Aglì G, Sglavo VM (2017) Rapid densification of samarium-doped ceria ceramic with nanometric grain size at 900–1100 °C. *Mater Lett* 190:17–19
- [29] Yavo N, Yeheskel O, Wachtel E, Ehre D, Frenkel AI, Lubomirsky I (2017) Relaxation and saturation of electrostriction in 10 mol% Gd-doped ceria ceramics. *Acta Mater* 144:411–418
- [30] Wang Z, Jiang S, Li Y, Xu P, Zhao K, Zong L, Wang H, Yu R (2017) Highly active CeO₂ hollow-shell spheres with Al doping. *Sci China Mater* 60(7):646–653
- [31] Moriana AD, Tian T, Sencadas V, Li W (2016) Comparison of rheological behaviors with fumed silica-based shear thickening fluids. *Korea-Aust Rheol J* 28(3):197–205